Maryami, R., Showkat Ali, S. A., Azarpeyvand, M., Dehghan, A., & Afshari, A. (2019). Experimental study of the unsteady aerodynamic loading for a tandem cylinder configuration. In *Proceedings of the 25th AIAA/CEAS Aeroacoustics Conference: 20-23 May 2019 Delft, The Netherlands* American Institute of Aeronautics and Astronautics Inc. (AIAA). https://doi.org/10.2514/6.2019-2742

Experimental study of the unsteady aerodynamic loading for a tandem cylinder configuration

Reza Maryami[1]
Yazd University, Yazd, Iran

Syamir Alihan Showkat Ali[2]
Universiti Malaysia Perlis, 02600 Perlis, Malaysia

Mahdi Azarpeyvand[3]
University of Bristol, Bristol, United Kingdom, BS8 1TR

Ali A. Dehghan[4]
Yazd University, Yazd, Iran

Abbas Afshari[5]
Yazd University, Yazd, Iran

An experimental study is carried out to investigate the unsteady aerodynamic loading on cylinders in tandem configuration in the sub-critical Reynolds number range. Experiments are performed using highly instrumented cylinders, with several static pressure taps and dynamic pressure transducers at different spanwise and peripheral locations. The effects of cylinders gap distance (L/D) on the static and dynamic surface pressure, coherence and turbulence length-scale have been investigated. The surface pressure results have shown a critical cylinders gap distances between $L/D = 3 - 3.7$, in which the flow patterns undergo an abrupt change in the reattachment and the co-vortex shedding regimes. For both cylinders, it is observed that the fundamental vortex shedding Strouhal number decreases with increasing L/D from 1.2 to 3, while for $L/D > 3$, the Strouhal number increases and approaches to that of the single cylinder model ($St \approx 0.2$). The spanwise coherence results have also shown that the vortex shedding structures have a high energy level and a long spanwise length scale, while the three-dimensional flow structures within the boundary layer have a much lower energy level and shorter correlation length. The existence of the broadband content of the spanwise coherence in the wake and especially close to the base of the cylinder is prominent at smallest cylinders gap distance ($L/D = 1.2$). Furthermore, the spanwise coherence at the peripheral angles close to the gap region is found to be purely tonal in the case of the downstream cylinder.

Nomenclature

B	=	wind tunnel blockage ratio
C_p	=	surface pressure coefficient
C_{p_b}	=	base pressure coefficient
D	=	cylinder diameter, m
f	=	frequency, Hz
f_0	=	fundamental vortex shedding frequency, Hz
f_1	=	first vortex shedding harmonic, Hz
f_2	=	second vortex shedding harmonic, Hz
f_{KH}	=	secondary vortex shedding frequency, Hz
L	=	cylinders gap distances, m

[1] Ph.D Student, School of Mechanical Engineering, *r.maryami@gmail.com*
[2] Senior Lecturer, School of Manufacturing Engineering, *syamir@unimap.edu.my*
[3] Reader in aeroacoustics, Department of Mechanical Engineering, *m.azarpeyvand@bristol.ac.uk*
[4] Associate Professor, School of Mechanical Engineering
[5] Ph.D Student, School of Mechanical Engineering

p = pressure fluctuations, Pa
p_∞ = freestream smooth flow pressure, Pa
Re = Reynolds number, $U_\infty D/v$
St = Strouhal number, fD/U_∞
U_∞ = free stream velocity, m/s
t = time, s
x, y, z = streamwise, normal and lateral distance coordinate, m
$\gamma^2_{p_i,p_j}$ = coherence function
η_z = spanwise microphone separation distance, m
θ = peripheral angle, deg.
θ_m = angular position of minimum pressure, deg.
θ_s = separation angle, deg.
θ_r = reattachment angle, deg.
Φ_{pp} = surface pressure power spectral density, Pa^2/Hz
Λ_{pp} = spanwise length scale, m
PSD = Power Spectral Density

I. Introduction

Rods in a crossflow exhibit periodic vortex shedding which produces a whistling sound. This sound is an unwanted effect of bluff bodies in a crossflow, which can be characterized as both tonal, due to the period aerodynamic forces acting on the cylinder which is due to the vortex shedding, and broadband, because of the presence of strong three-dimensional random fluctuations within the boundary layer and the near-wake. Bluff bodies appear in many engineering applications, for example, risers in marine engineering, buildings, bridges, tubular heat exchangers, power transmission lines, chimneys, towers, etc. and have been extensively studied over the recent years [1-4]. Naturally, some structures in a group are submerged in the wake of the others. Two inline cylinders may be considered as the basic element of multiple structures, where the downstream cylinder is in the wake of the upstream cylinder. The knowledge of this flow is insightful for understanding the flow around structures in groups.

In the tandem arrangement, Zdravkovich [5] and Igarashi [6] described the state of the flow interferences within the cylinders gap region according to the separation between the two cylinders. They explained that at the smallest separation distances, the free shear layers which separated from upstream cylinder do not reattach onto the downstream cylinder, but rather enclose it. As separation distance is increased, the flow becomes unpredictable as the wake-body-wake interactions intensify and the cylinders tend to have different shedding frequencies. At very large separation distances, the flow around the upstream cylinder closely resembles that of the single cylinder. There is an overlap in the specified separation distance ranges due to the Reynolds number effects, indicating that the location of transition also plays an equally important role in tandem cylinder flow. Lin *et al.* [7] performed experiments using PIV techniques in an attempt to characterize the flow features of two cylinders in tandem by controlling the separation distance. They found that in the gap region between the cylinders, small scale concentrations of vorticity formed in the separated shear layers which buffeted the surface of the downstream cylinder. This influenced the eventual shedding large-scale vortices. Experiments were performed by Jenkins *et al.* [8] to characterize the unsteady flow structures around tandem cylinders with a separation $L/D = 1.432$ and $L/D = 3.7$ at $Re = 1.66 \times 10^5$. It is observed that in the $L/D = 1.432$ case the cylinders together behaved much like a single bluff body since no vortices were shed from the upstream cylinder and the shear layer enclosed to the gap region. In the $L/D = 3.7$ configuration, vortices were shed from the upstream cylinder in the gap region. These vortices were shown to interact with the front surface of the downstream cylinder, leading to higher pressure fluctuations on its surface. The noise generated by tandem cylinders was also investigated experimentally by Hutcheson and Brooks [9]. Several configurations were investigated such as in-line cylinders with equal and none-equal diameters at a range of separation distances. For equal cylinders' diameter, a shift in the Strouhal number and peak SPL were observed relative to a single cylinder between $L/D = 1$ and $L/D = 4.5$. Detailed noise and surface pressure measurements were performed on tandem cylinder configurations by Hutcheson *et al.* [10]. They showed an increase in Strouhal number with L/D and no notable change in flow regime for all L/D and flow speeds. The results also highlighted the existence of higher peak and broadband noise levels for the smooth cylinder configurations.

For a proper understanding of the noise generation mechanism from external bodies in a flow, it is important to study the flow-field around the object and the unsteady forces exerted by flow structures. The most conventional and effective method for measuring the unsteady surface pressure fluctuations acting on the surface in a flow field is the use of miniature pressure transducers. Using such a method, one can obtain a reliable measurement of the unsteady

pressure over a wide range of frequencies. Unfortunately, there is no comprehensive study to investigate the surface pressure fluctuations over the circumference of the tandem cylinders and along their span. This paper aims to provide extensive body of research on the unsteady pressure exerted on the surface of circular cylinders in the tandem configuration in the subcritical flow regime and perform comprehensive near-field correlation studies to improve our understanding of the noise generation mechanisms from bluff bodies. The experimental setup and wind tunnel tests are described in Sec. II. The results and discussions are detailed in Sec. III.

II. Experimental setup

A. Wind tunnel and model

The experiments were carried out in the blowdown subsonic wind tunnel of the Yazd University with an exit cross-sectional area of $460\ mm \times 460\ mm$. The free-stream turbulence intensity at a maximum speed of 25 m/s was found to be less than 0.3%. The wind tunnel used in the present study has a centrifugal forward blades type fan with low broadband noise signature. To further improve the acoustic properties of the wind tunnel and avoid noise contamination due to the fan background noise, the internal solid surfaces of the tunnel were replaced with a highly absorbing porous layer [11], which resulted in the reduction of the fan background noise by about 15 dB over a wide range of frequencies.

The test model consists of two identical cylinders in tandem arrangement, aligned in a streamwise direction with a separation distance (center to center), L, ranging from 1.2 D to 6 D, where D is the cylinder diameter. The upstream cylinder was positioned at a fixed location on the nozzle centerline, while the downstream cylinder was moved in the streamwise direction to achieve the desired cylinders gap distances. Both cylinder models tested in the present work have an outer diameter of 22 mm and a span length of 460 mm. In order to simplify the instrumentation of the models with in-situ pressure sensors, each circular cylinder model is made of three parts, namely one middle section with the static and dynamic pressure instrumentations and two side parts to extend the span length of the model to that of the wind tunnel exit, as shown in Fig. 1. Both models have an aspect ratio (span-length to diameter) of over 20. The wind tunnel blockage ratio of the test rig is also less than 5 % and therefore the effects of blockage on pressure distribution and the Strouhal number can be assumed negligible [12]. Cylinders are placed within the potential core of the exiting jet flow and supported by two parallel rectangular end-plates downstream of the contraction nozzle. The models are properly fixed to the side-plates to eliminate the possibility of vibration. The cylinders are mounted on a turning-table to enable data collection using the static pressure taps and pressure transducers in fine angular increments. The details of the experimental setup are provided in Fig. 1.

B. Surface pressure instrumentation

Unsteady surface pressure measurements are made using Panasonic electret condenser pressure transducers (series WM-61A). The transducers have a diameter of 6 mm, height of 3.4 mm and circular sensing area of 2 mm. The same type of pressure transducers had previously been used in similar studies [13] and has shown to provide reliable pressure recording in the frequency range considered here. In order to reduce the attenuation effects at high frequencies, pressure measurements are made via a small pinhole at the surface of the cylinder [14-17]. Also, as reported by Bull and Thomas [18], the discontinuity on the surface of the model due to the presence of the pinholes can cause flow disturbance and errors in the measurement at high frequencies. Such errors can be minimized to a large extent by employing pinholes with very small diameters [19].

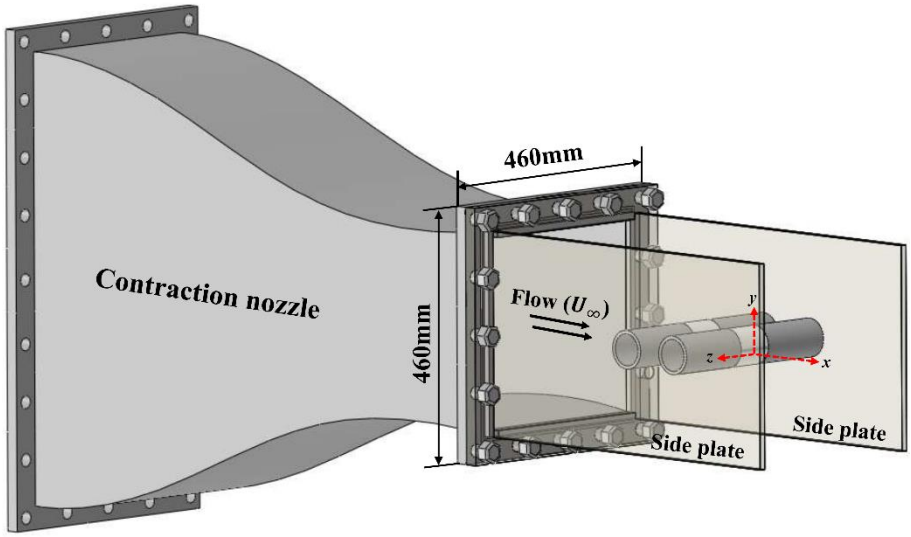

Fig. 1. The geometry of the contraction nozzle and tandem cylinders arrangement

As shown in Fig. 2, the pressure transducers are placed inside the cylinder, underneath a small pinhole mask of 0.55 mm diameter, and fixed in place using a fully sealed holding mechanism. The pinholes are made using an accurate drill machine. The geometrical dimensions of the pinholes and the pressure transducer holding mechanism are shown in Fig. 2. A more detailed explanation regarding the pressure transducers installation and calibration can be found in Refs [2, 20-22].

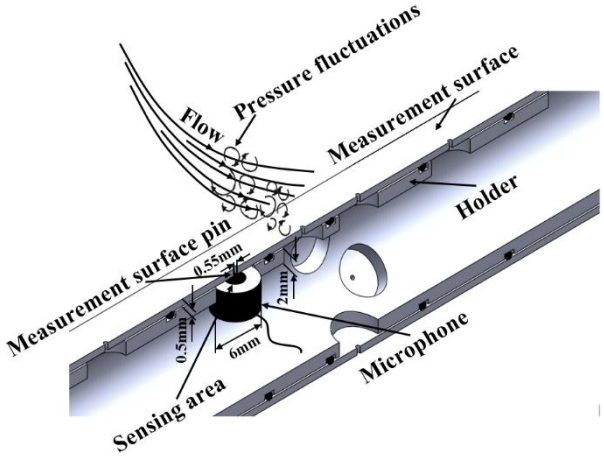

Fig. 2. In-situ boundary layer surface pressure measurement using a pressure transducer installed under a pinhole

C. The layout of surface microphone array

The layout of the pressure transducers used for the measurement of the dynamic pressure acting on the surface of the cylinder is depicted in Fig. 3. The locations of the pinholes are also summarized in Table 1. A total number of 15 microphones are distributed in the spanwise and peripheral directions. A set of microphones (p1-p8) are installed on a straight line along the span of the cylinder to verify the two-dimensionality of the flow and also to measure the

spanwise length-scale at different frequencies. To fully resolve the flow structures, the spanwise transducers must be distributed over at least 5D-7D, as reported in the literature [10, 13, 23]. At the same time, the transducers must be kept outside the boundary layer developed by the wind tunnel side-plates. The maximum thickness of the boundary layer created on the side-plates at the flow velocity of 20 m/s is found to be 8 mm. In this study, the pressure transducers are distributed over 6D (132 mm) along the span and are always outside the side-plate boundary layer. The minimum distance between the transducers is limited by the physical dimension of the transducers. The pinholes in the spanwise direction are distributed according to a potential function, with an unequal spacing, providing a non-redundant population of sensor spacing and a maximum number of spatial distances available for cross-correlation studies. Another set of pressure transducers (p9-p15) are distributed around the circumference of the model at the mid-span plane with an angular spacing of 45°, to provide information on the flow structures and shedding at different peripheral angles. The turning-table has been used to collect data at every 5° degrees. A 32-channel power module was used to power the Panasonic pressure transducers and the data were collected using two 16-channel NI PCI-6023E data acquisition systems. The sampling frequency used is $f_s = 40$ kHz, and a total of 800,000 samples were recorded over 20 s. Reliable and repeatable measurements are achieved for all pressure transducers. The uncertainty in the surface pressure spectra due to the statistical convergence error was about 3.5%.

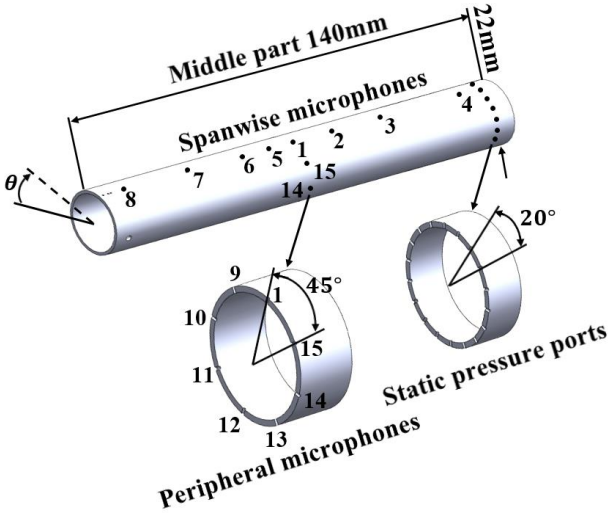

Fig. 3. The sensing area on the cylinder equipped with static pressure taps and spanwise and peripheral pressure transducers

Table 1. Position of pressure pinholes on the surface of the model

Microphones	z/D	θ (deg)	Microphones	z/D	θ (deg)
p1	0.0	90	p9	0.282	45
p2	0.682	90	p10	0.0	0.0
p3	1.545	90	p11	0.282	-45
p4	2.955	90	p12	0.0	-90
p5	-0.41	90	p13	0.282	-135
p6	-0.91	90	p14	0.0	180
p7	-1.864	90	p15	0.282	135
p8	-3.0	90	----	----	----

D. Static pressure measurement

In order to study the cylinder flow-field and measure the pressure distribution around the cylinder (C_p), the model is instrumented with 18 static pressure taps, distributed evenly with 20° spacing over the circumference of the cylinder, as shown in Fig. 3. The pressure taps have a diameter of 0.55 mm. Each tap-hole is tightly fitted with a 5 mm long brass tube, with the inner and outer diameters of 0.4 mm and 0.6 mm, respectively. The brass tubes are then connected to a series of polyurethane tubes with the diameters of 1mm, 3 mm and 4 mm, and finally connected to the pressure scanner ports outside the cylinder. The static pressure measurements are carried out using a Honeywell electronic differential pressure measurement unit with 32 channels with a range of ± 1.25 kPa. An uncertainty analysis of the pressure measurement, based on the method described in Ref. [24], showed a maximum uncertainty of 2.2%.

III. Results and Discussion

A. Aerodynamic characteristics

The pressure coefficient distribution around the two cylinders in tandem at $Re = 14.7 \times 10^3$, 22×10^3 and 30×10^3, based on the diameter of the cylinder is presented in Fig. 4 for five different cylinders gap distances. This Reynolds number range is limited to the subcritical regime, as reported by [25]. The results show that the mean pressure coefficient on the upstream cylinder is similar for all cylinders gap distances and Reynolds numbers. The differences are observed mainly in the wake region. The overall trend of the distributions is also similar to that of the single cylinder. The pressure coefficient of the upstream cylinder is maximum ($C_p \approx 1$) at the stagnation point ($\theta = 0°$) but decreases to a minimum point at $\theta_m = 70°$, which is also the starting point of the adverse pressure gradient region. For $\theta > 70°$, the increase in the pressure coefficient occurs and the laminar boundary layer separation can ultimately be seen at $\theta_s = 80°$. In the base pressure region, which extends from the separation point (θ_s) to the base of the cylinder ($\theta_b = 180°$), nearly constant pressure can be observed, consistent with the results of a single cylinder. In general, it can be seen that at all Reynolds number there are certain effects of the downstream cylinder on the pressure distribution of the upstream one, essentially on the values of minimum pressure (C_{p_m}) and of the base pressure (C_{p_b}), *i.e.* C_p at $\theta_b = 180°$. These effects are relatively stronger at subcritical Reynolds number than at supercritical one [26]. Depending on the Reynolds number value, the pressure distribution results of the upstream cylinder indicate an increase in the pressure coefficient value as the cylinders gap distance increases from $L/D = 1.2$ to $L/D = 3 - 3.7$. This is true for all angular positions around the upstream cylinder but is prominent in the base pressure region. For cylinders gap distances limited to $L/D > 3 - 3.7$, the opposite trend can be seen, and the minimum pressure coefficient takes place at the largest cylinders gap distance, *i.e.* $L/D = 6$. The more interesting issue, however, is that the pressure distribution of the upstream cylinder for $L/D = 6$ presents a similar curve to the one for single cylinder because the separated shear layer from upstream cylinder rolls up in the gap between cylinders in addition to the wake of the downstream cylinder. For $L/D = 1.2$ and 1.432, where the gap is believed to contain mostly stagnant fluid [5] or oscillatory cavity-flow-type behavior [27] and the flow predominantly consists of vortex shedding behind the downstream cylinder, the pressure distribution curves are similar to that of the single cylinder. Note that for small gap cylinders gap distances up to $L/D = 3 - 3.7$, the base pressure coefficients of the upstream cylinder (C_{p_b}) are almost the same as the pressure coefficient of the front stagnation point of the downstream cylinder. This fact can be due to the quasi-stationary vortices formed in the gap between cylinders [6, 28].

On the downstream cylinder, the variations in C_p are larger as the cylinders gap distances are changed, which is clearly seen in Fig. 4. This, of course, makes sense as the pressure distribution on the downstream cylinder is dependent on the state of the gap flow. Up to the critical cylinders gap distances $L/D = 3 - 3.7$, there is a strong low negative pressure near the stagnation point in the pressure distribution around the downstream cylinder. In this cylinders gap distance range, it can also be seen that pressure reaches a maximum value at the position of reattachment point (θ_r), where the separated shear layer from upstream cylinder reattaches onto the downstream cylinder. Generally, the reattachment position is shifted to the front stagnation point with increasing cylinders gap. It should be noted that the shear layer reattachment behavior leads to a backward shift in angular position of the minimum pressure and boundary layer separation on the downstream cylinder, *i.e.*, respectively, $\theta_m = 100°$ and $\theta_s = 140°$. In the case of $L/D = 6$, the minimum pressure coefficient is found to be 70°, while the separation occurs at $\theta_s \approx 140°$. For all the Reynolds numbers except $Re = 14.7 \times 10^3$, the base pressure coefficient in the case of the downstream cylinder decreases to $C_{p_b} \approx -0.57$ at $L/D = 3.7$ and then increases for $L/D > 3.7$. The same trend can be seen for $Re = 14.7 \times 10^3$, but increase in the base pressure coefficient begins from the critical cylinders gap distance of 4D. For both cylinders, a decrease in the base pressure is due to the increased curvature of the free streamline and entrainment of reversed flow into the opposing shear layer which corresponds to the reduction of the vortex formation length and enhancement of the diffusion length [29]. In this case, an increase in the vortex strength is expected.

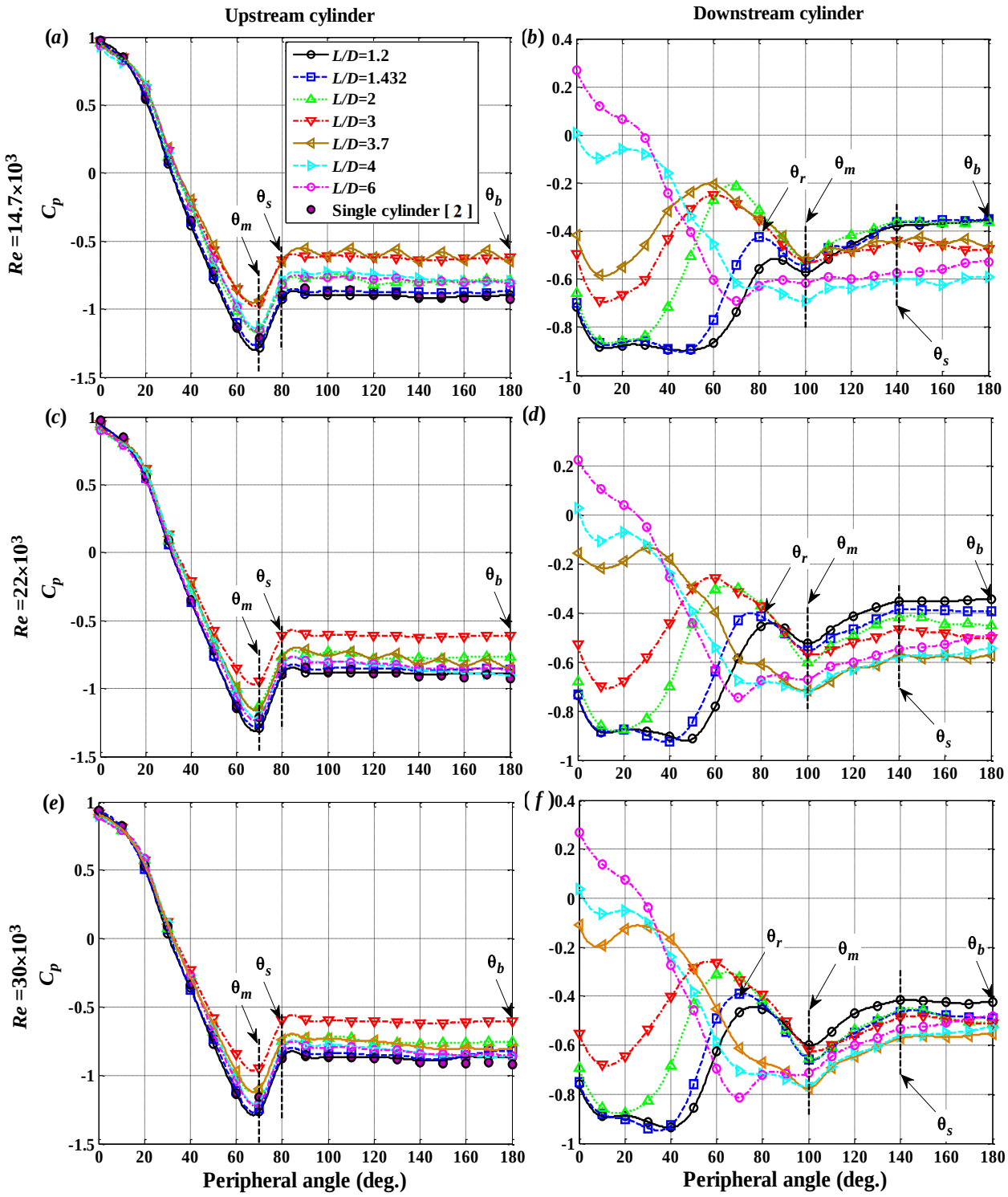

Fig. 4. Mean pressure coefficient distributions around the front and rear cylinders.

B. Boundary layer surface pressure fluctuations

The power spectral density of the surface pressure fluctuations (PSD) obtained from the pressure transducers p1, p9, p10, p14 and p15 for both the upstream and downstream cylinders at $Re = 30 \times 10^3$ are presented in Figs. 5 and 6, respectively. In order to estimate the energy content at different frequencies, the Welch's power spectral density of pressure fluctuations (ϕ_{PP}) has been performed based on the time-domain pressure transducer data in Matlab using Hamming windowing for segments of equal length with 50% overlap. The frequency resolution was set to 64 Hz. The pressure PSD data are referenced to 20 μPa. The PSD results are presented only when the surface pressure fluctuations are at least 10dB higher than the background noise due to the freestream flow. The fundamental, first and second harmonics of the vortex shedding frequency (*i.e.*, f_0, $f_1 = 2f_0$ and $f_2 = 3f_0$, respectively) can be clearly seen from the results of both cylinders. The strong tonal behavior observed is associated with the fundamental frequency, which can be attributed to the presence of a strong hydrodynamic field travelling upstream from the wake region, where flow recirculation occurs, for both the cylinders. It can be inferred that the flow structures corresponding to this field, *i.e.* Von Karman vortices, play a major role in generating surface pressure fluctuations exerted on tandem cylinders. This tonal peak is detected for almost all cylinders gap distances and angular positions, except $L/D \geq 3$ in the case of upstream cylinder base ($\theta = 180°$) as shown in Fig. 5. Interestingly, for the downstream cylinder at $L/D \geq 3.7$, in addition to $\theta = 180°$, at front stagnation point ($\theta = 0°$) tonal peak at the f_0 have very small amplitude compared to that of the f_1. As can be observed, the reduction of the broadband content of the surface pressure PSD with frequency is significant and consistent for both the cylinder cases. The decay gradient of the surface pressure spectra after the second harmonic, however, changes with the angle and it is prominent for the upstream cylinder. At large angles ($\theta = 135°$ and 180°), and particularly at the cylinder base ($\theta = 180°$), the surface pressure PSD spectra follow a smaller gradient than that of the small angles ($\theta = 0°$, 45° and 90°). This trend is completely reversed for the downstream

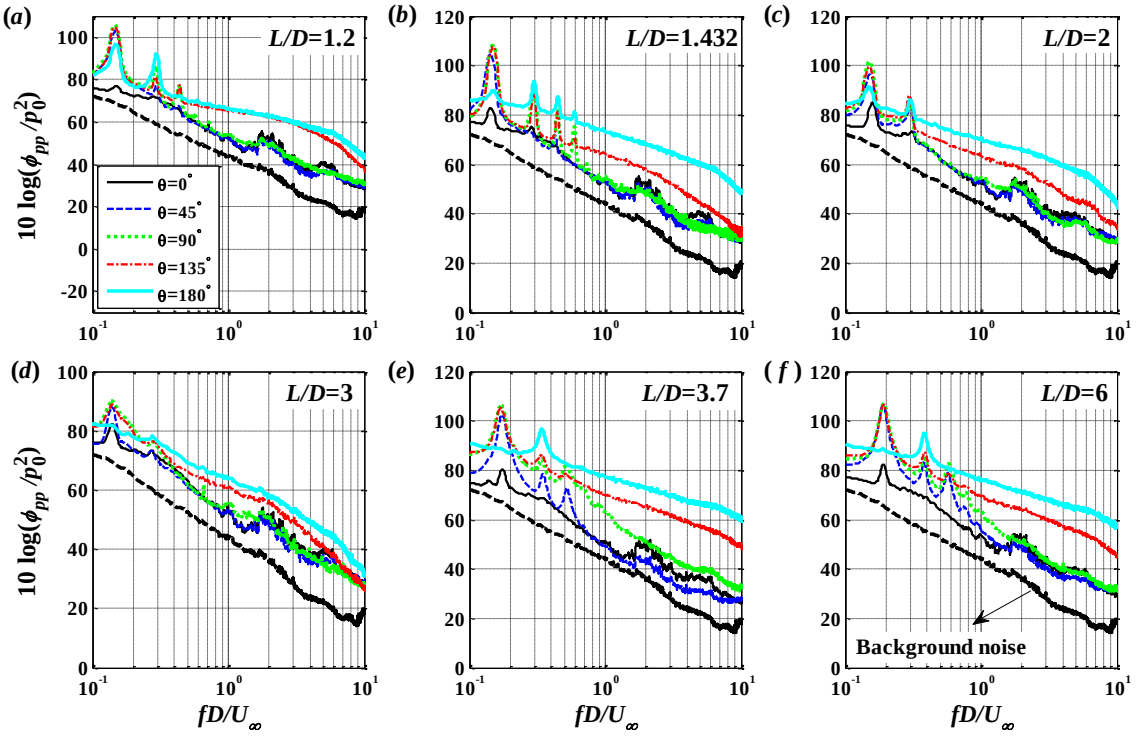

Fig. 5. Surface pressure power spectral density measured at different angular positions at $Re = 30 \times 10^3$ for the upstream cylinder at different cylinders gap distances (L/D).

cylinder. It is noticeable that the difference between the PSD spectra gradients at different angles for the upstream cylinder is considerably higher than those of the downstream one. Moreover, the reduction in the broadband content of the energy spectra in the case of both cylinders has made the tones to protrude well above the broadband spectra. Another important issue is that for the upstream cylinder, the broadband content of the PSD spectra increases over the angle in the whole Strouhal range. In the case of the downstream cylinder, a lower level of the PSD broadband content is monitored at $\theta = 180°$, while depending on L/D and the ranges of Strouhal number, the highest PSD level for this

component occurs at one of the angles of $\theta = 45°$, 90° and 135°. Generally, the difference between the broadband levels at different angles around the downstream cylinder are prominent within $1.2 \leq L/D < 3$, as shown in Fig. 6.

A fact that would require further attention is that beyond $St = 6$ in upstream cylinder case, the surface pressure PSD nearly tends to increase for angles of $\theta = 45°$ and 90°, while experimental data at $\theta = 135°$ and 180° show sharp decreases with Strouhal number. The rise in the surface pressure fluctuations at forward angles (*i.e.* $\theta = 45°$ and 90°) is believed to be partly due to the transition to the turbulent flow and the observations of sudden drop in PSD at rearward angles (*i.e.* $\theta = 135°$ and 180°) also reflect the effects of the instabilities in the separated boundary layer immediately downstream of the separation point. As established by Wei and Smith [30], the so-called secondary vortices are the result of the amplification of these instabilities which play a major role in the transition to turbulence. The vortices in the separated boundary layer are small-scale vortices which grow up and feed the large-scale Karman vortices. However, the effect of the base pressure fluctuations in the vicinity of the rear stagnation point is undeniable in generation of the Strouhal vortices [31]. As has been shown, for $St > 6$, the PSD enhancement ceases to occur at all angles around downstream cylinder because the presence of upstream cylinder, similar to the upwind turbulence-generating grids, leads to flow on downstream one becomes entirely turbulent. The effects of free shear layer instabilities on the surface pressure PSD, on the other hand, can be seen with broadband hump around $St \approx 7$ at all cylinders gap distances and angular positions. Note that in the downstream cylinder case, at the pre-separation angles ($\theta < \theta_s \approx 100°$), the broadband hump can be due to the effects of instabilities in free shear layers separated from

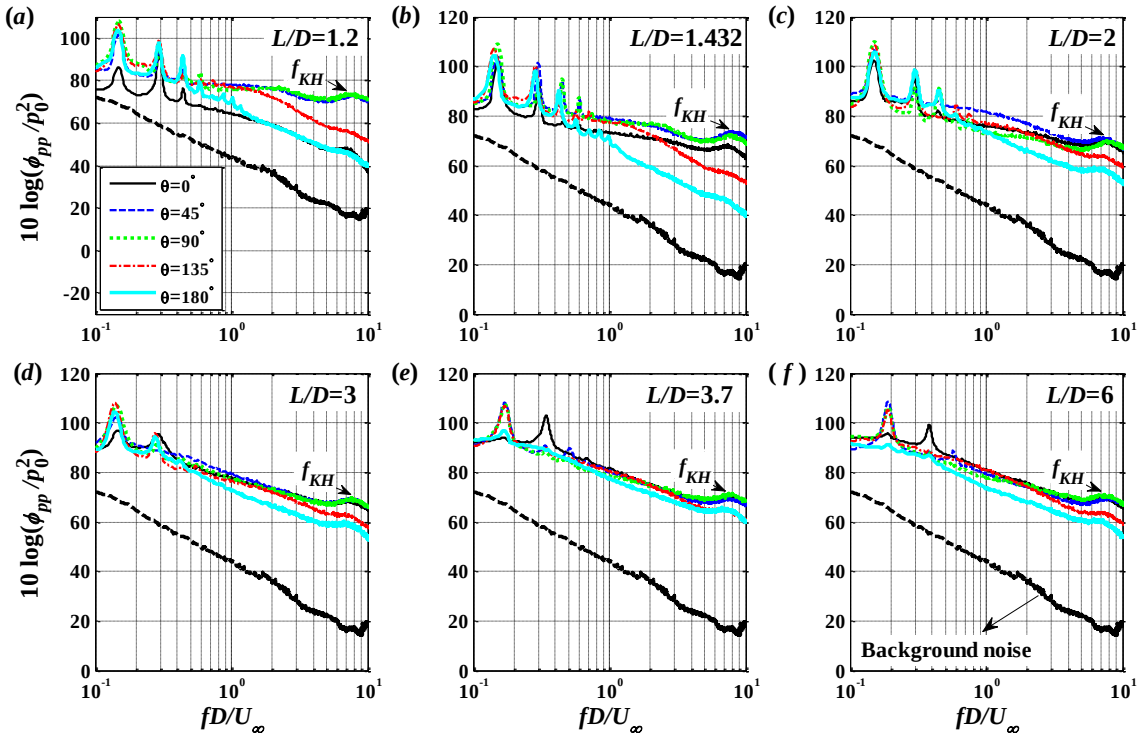

Fig. 6. Surface pressure power spectral density measured at different angular positions at $Re = 30 \times 10^3$ for the downstream cylinder at different cylinders gap distances (L/D).

upstream cylinder, while at post separation angles ($\theta > \theta_s \approx 100°$), the broadband hump is dominantly sensitive to formation of secondary vortices in the boundary layer separated from downstream cylinder. According to Ref. [30], non-dimensional secondary vortex shedding frequency (f_{KH}) is related to the Karman vortex shedding frequency (f_0) and Reynolds number through the expression $f_{KH}/f_0 = (Re/470)^{0.87}$. The dependency of f_{KH}/f_0 with Reynolds confirmed by other researchers (*e.g.* $f_{KH}/f_0 \propto Re^{0.67}$ by Prasad and Williamson [32], $f_{KH}/f_0 \propto Re^{0.68}$ by Norberg [33] and $f_{KH}/f_0 \propto Re^{0.69}$ by Thompson and Hourigan [34]).

C. Pressure coherence analysis

The results in section B showed the changes to the surface pressure PSD and the vortex shedding frequencies at different peripheral angles and cylinders gap distances. The results demonstrated that the energy content of the boundary layer and wake turbulence structures changes with L/D and the angular positions around the cylinders, leading to significant changes to the boundary layer and the wake flow field. In this section, we will further investigate the changes to the shape of the flow structures corresponding to the boundary layer and vortex formation region by studying the lateral coherence of the surface pressure signals over the surface of both cylinders. These results will enable us to better understand the underlying physics of boundary layer structures convected downstream and the hydrodynamic energy travelling upstream from the vortex shedding region.

1. Surface pressure lateral coherence and length scale

The lateral coherence of the turbulent structures and their corresponding length scale have been studied using the pressure transducers (p1-p8). The coherence between pressure transducers along the span the lateral length scale can be found from,

$$\gamma^2_{p_i p_j}(\eta_z, f) = \frac{\left|\Phi_{p_i p_j}(\eta_z, f)\right|^2}{\Phi_{p_i p_i}(\eta_z, f)\Phi_{p_j p_j}(\eta_z, f)} \tag{1}$$

and

$$\Lambda_{pp}(f) = \int_0^\infty \sqrt{\gamma^2_{p_i p_j}(f, \eta_z)}\, d\Delta z, \tag{2}$$

where $\Phi_{p_i p_j}(\eta_z, f)$ denotes the cross-spectrum between the two pressure signals, $\Phi_{p_i p_i}(\eta_z, f)$ is the auto-spectrum of each individual signal, and η_z is the spanwise separation distance between the transducers.

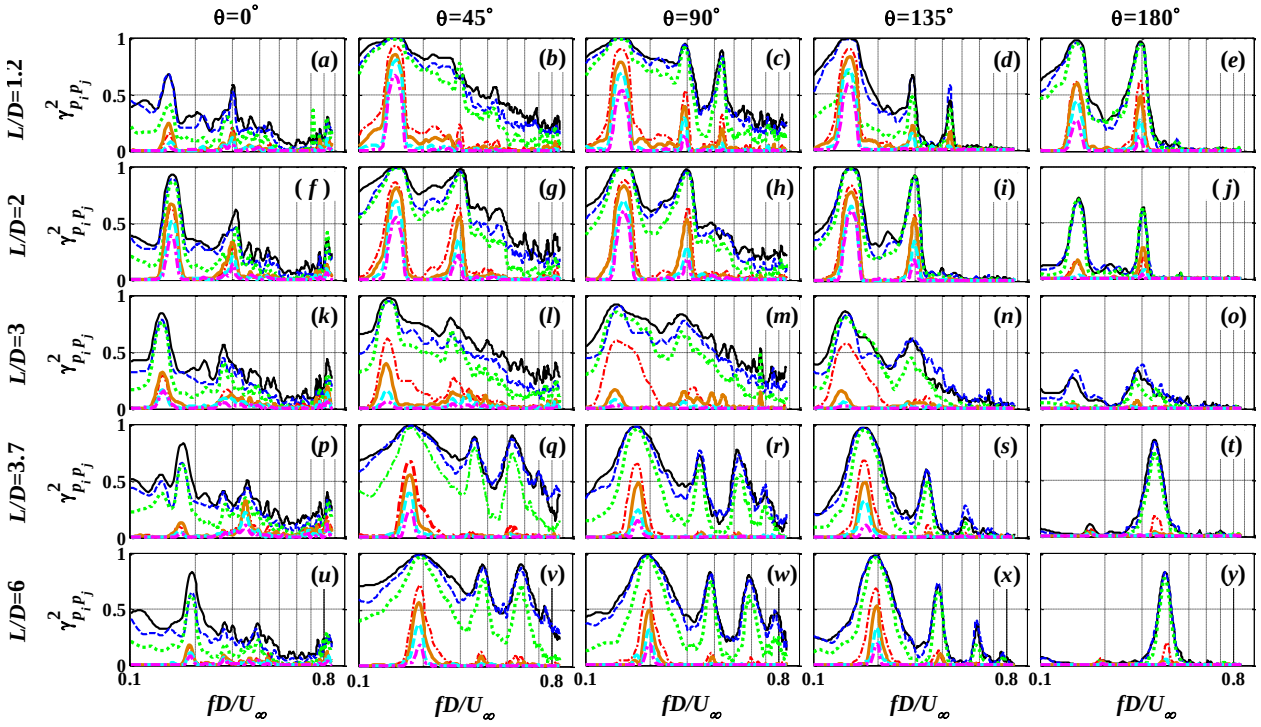

Fig. 7. Lateral coherence measured around the upstream cylinder at $Re = 30 \times 10^3$ and at different cylinders gap distances (L/D). $\eta_z/D = 0.41$(——), $\eta_z/D = 0.5$ (- - - - -), $\eta_z/D = 0.68$ (·····), $\eta_z/D = 2.27$(-·-·-·), $\eta_z/D = 3.41$(——), $\eta_z/D = 4.54$(- - - - -), $\eta_z/D = 5.95$(-··-··-).

For the upstream and downstream cylinder, respectively, Figs. 7 and 8 present the lateral coherence measured between the spanwise transducers for the lateral spacings in the range of $\eta_z/D = 0.41$ to 5.95, which should be sufficient for capturing the two- and three-dimensional flow structures. The coherence ($\gamma^2_{p_i p_j}$) results are plotted as a function of the Strouhal number (fD/U_∞) at $Re = 30 \times 10^3$ for both the upstream and downstream cylinders with a center to center cylinders gap distance range of $1.2 \leq L/D \leq 6$. In all cases, as expected, a strong coherence can be observed at the vortex shedding frequencies (f_0, f_1 and f_2) between the pressure signals. Moreover, the lateral coherence value at the fundamental frequency is greater than those at f_1 and f_2, except for $\theta = 180°$ at $L/D \geq 3$ in the case of the upstream cylinder and $\theta = 0°$ nearly between $L/D = 1.2 - 6$ in the case of the downstream cylinder. The results clearly show that different distances of η_z/D and L/D have a significant and distinct effect on the lateral coherence of the flow structures, depending on the angular positions around the tandem cylinders. It can be generally observed that the lateral coherence level between the transducers decreases with η_z/D at all angles. The coherence at the small lateral spacings close to the range of $\eta_z/D = 0.41 - 0.68$, has a relatively strong broadband content, in addition to the distinct strong peaks at f_0, f_1 and f_2. With increasing the spanwise separation distance, however, the tonal components have only appeared, and the lateral coherence entirely becomes zero at other frequencies. It can be concluded that coherence level of the three-dimensional flow structures is small within a short lateral distance (between $\eta_z/D = 0.68 - 2.27$), while the two-dimensional structures, *i.e.* vortex shedding structures, retain their coherence over a much longer spanwise distance. This clearly indicates that the physical size of the two-dimensional structures is considerably large and their role in generating surface pressure exerted on cylinders is very significant.

In the case of the upstream cylinder, the coherence results at the stagnation point ($\theta = 0°$) show a broadband behavior with tonal peaks at the f_0 and f_1, indicating that the hydrodynamic field due to the Karman vortex shedding can be realized at the stagnation point. The broadband content of the coherence is particularly strong at $\theta = 45°$ and then decreases with angles. This is valid for all the cylinders gap distances, except for the smaller one, *i.e.* $L/D = 1.2$. At pitch ratio of $1.2D$, the downstream cylinder places inside the vortex formation region of the upstream cylinder and the separated shear layers from the upstream cylinder are forced to reattach onto the downstream cylinder (see Fig. 4) before rolling up into the Karman vortices behind the downstream cylinder. Both the cylinders, in this case, behave

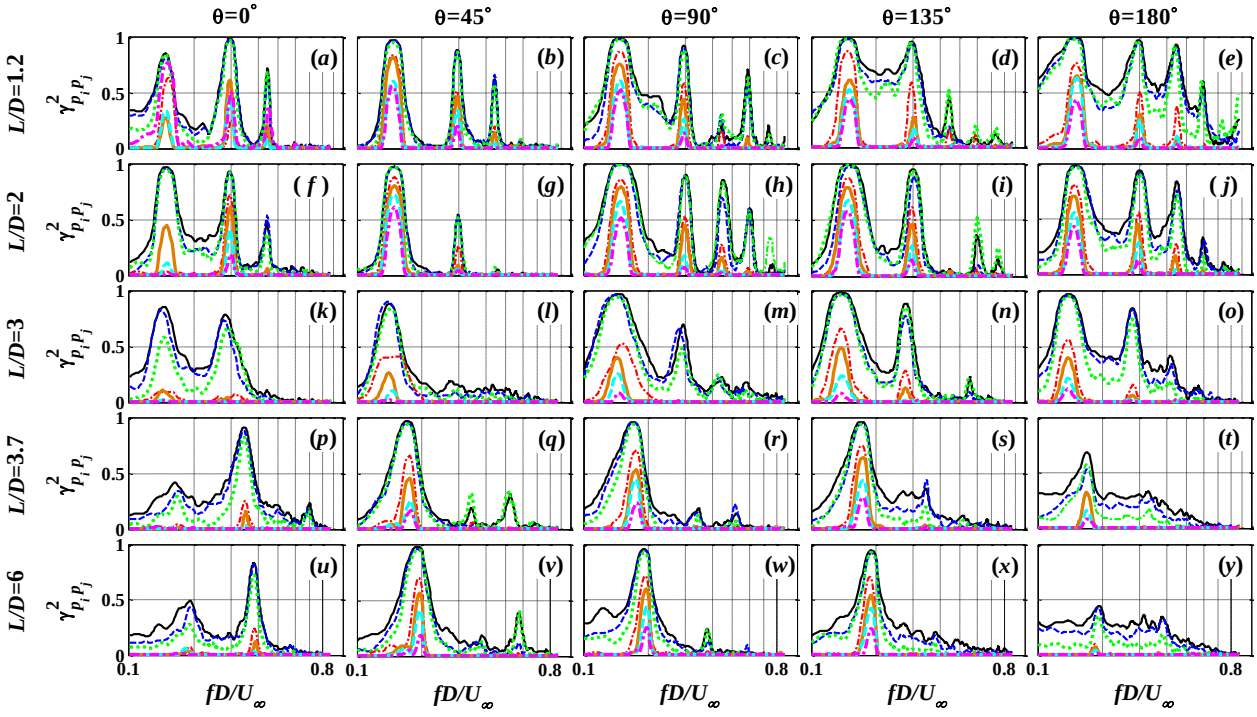

Fig. 8. Lateral coherence measured around the downstream cylinder at $Re = 30 \times 10^3$ and at different cylinders gap distances (L/D). $\eta_z/D = 0.41$(——), $\eta_z/D = 0.5$ (- - - -), $\eta_z/D = 0.68$ (·····), $\eta_z/D = 2.27$(-·-·-·), $\eta_z/D = 3.41$(——), $\eta_z/D = 4.54$(- - - -), $\eta_z/D = 5.95$(-·-·-·).

as an extended body that the shear layers from the upstream cylinder elongate considerably along the streamwise direction, where the three-dimensional structures have enough time to grow on the upstream cylinder and produce high broadband energy content region. The broadband content of the lateral coherence decreases with increasing L/D, except at $\theta = 0°$, which is prominent in the gap region and especially at the base of the upstream cylinder ($\theta = 180°$). This can be due to an upward shift in the vortex formation region with increasing cylinders gap distances in the gap region. At $\theta = 180°$, the lateral coherence is entirely tonal at f_0 for all pitch ratios except $L/D = 6$, that the maximum fundamental frequency amplitude ($\gamma^2_{p_i p_j} \cong 1$) can be observed at $L/D = 1.2$ between $\eta_z/D = 0.41 - 0.68$. tone at $\theta = 180°$.

In the case of the downstream cylinder, the lateral coherence is considerably dominated by tonal peaks at the vortex shedding frequencies for all spanwise distances as shown in Fig. 8, particularly, at the front stagnation point ($\theta = 0°$) and angles closer to the shear layers reattachment positions ($\theta = 45°$ and $90°$) compared to that of the upstream cylinder. It is believed that these tonal characters can be due to the emergence of a strong upstream-moving hydrodynamic field due to the vortex shedding behind the downstream cylinder, covering forward angular positions of the downstream cylinder. For all pitch ratios, the lateral coherence results observed at $\theta = 0°$ in the downstream cylinder case is nearly similar to those of the upstream cylinder at $\theta = 180°$. This is particularly an interesting result as it shows that the turbulent structures close to the gap region generate pressure fluctuations at the base of the upstream cylinder and front stagnation point of the downstream cylinder which correlate in a similar way at the spanwise direction. However, at $L/D = 6$, the emergence of the fundamental tone over a small spanwise distance range (*i.e.* from $\eta_z/D = 0.41$ to 0.68) at the front impingement point of the downstream cylinder is significant, while the lateral coherence at f_0 is completely eliminated at the base of the upstream cylinder. Note that for the downstream cylinder at the pitch ratio of 6D, the lateral coherence of the turbulent structure decays quickly with frequency after the fundamental tone at $\theta = 45°$, $90°$ and $135°$. The pressure signals measured by the spanwise transducers at $\theta = 180°$, in this cylinders gap distances, also exhibit much lower coherence values at f_0 and broadband content at other frequencies which is in contrast to the upstream and single cylinder cases. Another interesting phenomenon observed here is the emergence of a double-peak coherence behavior near f_0 at angles $\theta = 90°$ and 45 between $\eta_z/D = 2.72$ and 4.54 can be observed at $L/D = 4$ and 6 for both cylinders. A similar observation was made by Maryami *et al.* [2] for a single cylinder at angles of $\theta = 90°$ and $135°$. The nature of the double-peak is not quite clear and requires further investigation.

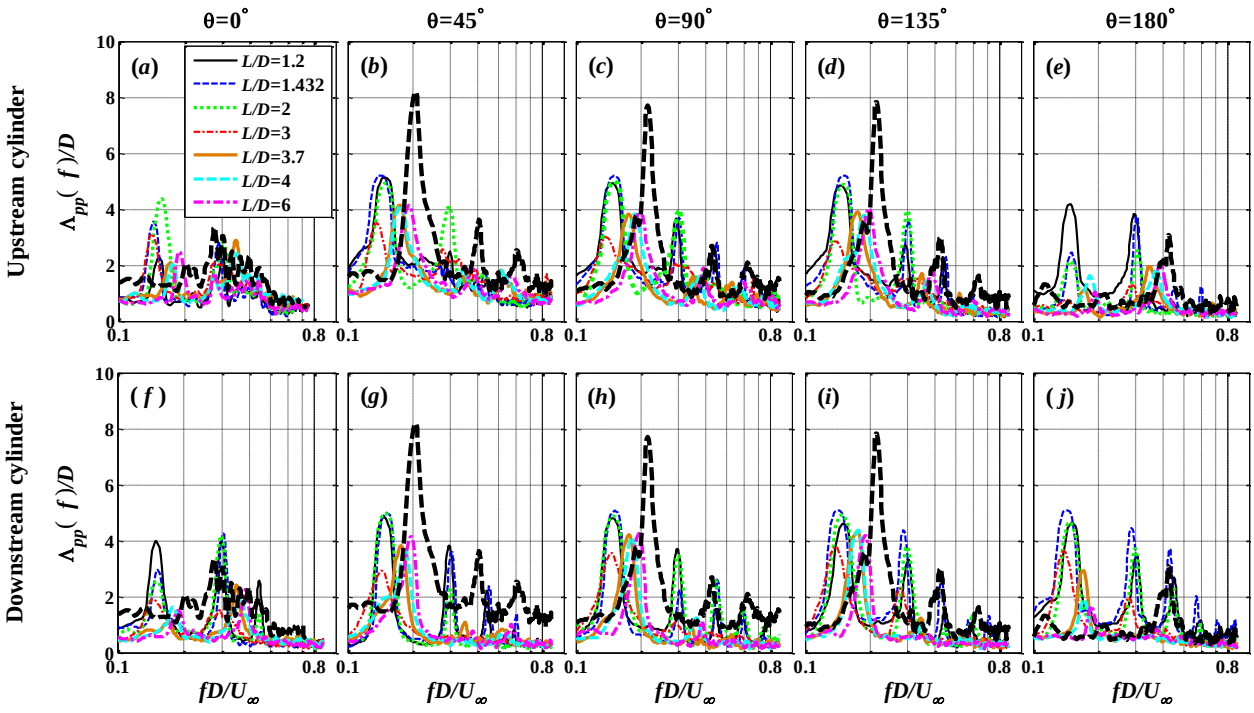

Fig. 9. Frequency-dependent spanwise length-scales of the surface pressure fluctuations at different angular positions at $Re = 30 \times 10^3$ for the upstream and downstream cylinders at different cylinders gap distances (L/D), Single cylinder [2] (▬ ▬ ▬)

Figure 9 shows the frequency dependent spanwise length-scale results (Λ_{pp}) calculated using Eq.2, based on the coherence of the pressure fluctuations between the spanwise transducers. In this figure, the results of tandem cylinders at $Re = 30 \times 10^3$ are compared against the single cylinder data [2]. In the case of both cylinders, the spanwise correlation length for $\theta = 45°$, 90° and 135°, experience a similar trend with distinct peaks at the fundamental vortex shedding frequency (f_0) and its harmonics f_1 and f_2, consistent with the results of a single cylinder. The results also show that the value of the spanwise length-scale at the fundamental frequency for these angles reaches about $\Lambda_{pp}(f_0) = 5D$ at $L/D = 1.2 - 2$, while that for $L/D = 3$ becomes nearly $\Lambda_{pp}(f_0) = 3D$ and again increases to $\Lambda_{pp}(f_0) \approx 4D$ at $L/D = 3.7 - 6$. The correlation length results for upstream and downstream cylinders at angles close to the gap region show nearly similar behavior at all pitch ratios. As can be observed in Fig. 9, at angles of 45°, 90° and 135°, the f_0- peak value of the spanwise length-scale in single cylinder case is larger than that of the tandem cylinders and their difference reaches a maximum at $L/D = 3$. At these angular positions, the difference between the spanwise length-scale for the single and tandem cylinder cases is prominent within $L/D = 3 - 6$. On the contrary, at $\theta = 180°$ and for all cylinders gap distances, both the upstream and downstream cylinders exhibit much larger spanwise length-scale at the fundamental frequency compared to that of the single cylinder. At largest pitch ratio ($L/D = 6$), as mentioned before, the tonal and broadband contents of the lateral coherence for the upstream cylinder case is similar to that of the single cylinder results of Ref. [20].

IV. Conclusion

The unsteady aerodynamic loading for a tandem cylinder configuration has been studied experimentally. Two identical circular cylinder models equipped with several peripheral and spanwise surface pressure microphones were used to measure the surface pressure fluctuations. The unsteady surface pressure interaction between the two cylinders in tandem was characterized by changing the cylinders gap distances. For both cylinders, results have shown the emergence of the fundamental, first and second harmonics at most of the peripheral angles. The broadband components, due to the boundary layer and wake flow structures generated around the cylinder can be seen from the onset of the boundary layer for the upstream cylinder and after the reattachment location around the downstream cylinder. The spanwise coherence results have also shown that the vortex shedding structures have a long spanwise length, while the three-dimensional flow structures have much shorter correlation length. The spanwise coherence at the peripheral angles close to the gap region for the rear cylinder is found to be purely tonal. The results in this paper provide a high-quality fundamental study on the unsteady aerodynamic loading for a tandem cylinder's configuration and provide the motivation for further numerical investigation in the context of noise generation mechanisms of bodies in tandem.

References

[1]Liu, H., Azarpeyvand, M., Wei, J. and Qu, Z. " Tandem cylinder aerodynamic sound control using porous coating," *Journal of Sound and Vibration* Vol. 334, 2015, pp. 190-201.

[2]Maryami, R., Azarpeyvand, M., Dehghan, A. A., and Afshari, A. "An Experimental Investigation of the Surface Pressure Fluctuations for Round Cylinders," *Journal of Fluids Engineering* Vol. 141, No. 6, 2018, pp. 061203-061203-11.

[3]Showkat Ali, S. A., Liu, X. and Azarpeyvand. " Bluff body flow and noise control using porous media," *22nd AIAA/CEAS Aeroacoustics Conference*, AIAA 2016-2754.

[4]Showkat Ali, S. A., Azarpeyvand, M. and da Silva, C. R. I. "Trailing Edge Bluntness Flow and Noise Control Using Porous Treatments," *22nd AIAA/CEAS Aeroacoustics Conference, AIAA 2016-2832.*

[5]Zdravkovich, M. "Flow induced oscillations of two interfering circular cylinders," *Journal of Sound and Vibration* Vol. 101, No. 4, 1985, pp. 511-521.

[6]Igarashi, T. "Characteristics of the flow around two circular cylinders arranged in tandem: 1st report," *Bulletin of JSME* Vol. 24, No. 188, 1981, pp. 323-331.

[7]Lin, J.-C., Yang, Y., and Rockwell, D. "Flow past two cylinders in tandem: instantaneous and averaged flow structure," *Journal of Fluids and Structures* Vol. 16, No. 8, 2002, pp. 1059-1071.

[8]Jenkins, L., Khorrami, M., Choudhari, M., and McGinley, C. "Characterization of unsteady flow structures around tandem cylinders for component interaction studies in airframe noise," *11th AIAA/CEAS Aeroacoustics Conference*. 2005, p. 2812.

[9]Hutcheson, F. V., and Brooks, T. F. "Noise radiation from single and multiple rod configurations," *International Journal of Aeroacoustics* Vol. 11, No. 3-4, 2012, pp. 291-333.

[10]Hutcheson, F. V., Brooks, T. F., Lockard, D. P., Choudhari, M. M., and Stead, D. J. "Acoustics and Surface Pressure Measurements from Tandem Cylinder Configurations," *20th AIAA/CEAS Aeroacoustics Conference*. 2014, p. 2762.

[11]Garcia-Sagrado, A., and Hynes, T. "Wall pressure sources near an airfoil trailing edge under turbulent boundary layers," *Journal of Fluids and Structures* Vol. 30, 2012, pp. 3-34.

[12]West, G., and Apelt, C. "The effects of tunnel blockage and aspect ratio on the mean flow past a circular cylinder with Reynolds numbers between 10 4 and 10 5," *Journal of Fluid Mechanics* Vol. 114, 1982, pp. 361-377.

[13]Wilkins, S. J., and Hall, J. W. "Experimental investigation of a tandem cylinder system with a yawed upstream cylinder," *Journal of Pressure Vessel Technology* Vol. 136, No. 1, 2014, p. 011302.

[14]Corcos, G. "Resolution of pressure in turbulence," *The Journal of the Acoustical Society of America* Vol. 35, No. 2, 1963, pp. 192-199.

[15]Goody, M. "Empirical spectral model of surface pressure fluctuations," *AIAA Journal* Vol. 42, No. 9, 2004, pp. 1788-1794.

[16]Showkat Ali, S. A., Azarpeyvand, M. and da Silva, C. R. I. " Trailing-edge flow and noise control using porous treatments," *Journal of Fluid Mechanics, Cambridge University Press, 2018, 850, 83-119*.

[17]Showkat Ali, S. A., Azarpeyvand, M. and da Silva, C. R. I. " Experimental Study of Porous Treatment for Aerodynamic and Aeroacoustic Purposes," *23rd AIAA/CEAS Aeroacoustics Conference, AIAA 2017-3358*.

[18]Bull, M., and Thomas, A. "High frequency wall-pressure fluctuations in turbulent boundary layers," *The Physics of Fluids* Vol. 19, No. 4, 1976, pp. 597-599.

[19]Goody, M. "An Experimental Investigation of Pressure Fluctuations in Three-Dimensional Turbulent Boundary Layers." Virginia Tech, 1999.

[20]Afshari, A., Azarpeyvand, M., Dehghan, A. A., and Szoke, M. "Effects of Streamwise Surface Treatments on Trailing Edge Noise Reduction," *23rd AIAA/CEAS Aeroacoustics Conference*. American Institute of Aeronautics and Astronautics, 2017.

[21]Showkat Ali, S. A., Azarpeyvand, M., Szoke, M. and da Silva, C. R. I. " Boundary layer flow interaction with a permeable wall," *Physics of Fluids, AIP Publishing, 2018, 30, 085111*.

[22]Showkat Ali, S. A., Szoke, M., Azarpeyvand, M. and da Silva, C. R. I. " Turbulent Flow Interaction with Porous Surfaces," *24th AIAA/CEAS Aeroacoustics Conference, AIAA 2018-2801*.

[23]Fujita, H., Suzuki, H., Sagawa, A., and Takaishi, T. "The Aeolian tone and the surface pressure in high Reynolds number flow," *6th Aeroacoustics Conference and Exhibit*. 2000, p. 2002.

[24]Yavuzkurt, S. "A guide to uncertainty analysis of hot-wire data," *Journal of Fluids Engineering* Vol. 106, No. 2, 1984, pp. 181-186.

[25]Zdravkovich, M. "Flow around circular cylinders volume 1: fundamentals," *Oxford University Press, Oxford* Vol. 19, 1997, p. 185.

[26]Sun, T., Gu, Z., He, D., and Zhang, L. "Fluctuating pressure on two circular cylinders at high Reynolds numbers," *Journal of Wind Engineering and Industrial Aerodynamics* Vol. 41, No. 1-3, 1992, pp. 577-588.

[27]Hetz, A., Dhaubhadel, M., and Telionis, D. "Vortex shedding over five in-line cylinders," *Journal of Fluids and Structures* Vol. 5, No. 3, 1991, pp. 243-257.

[28]Ljungkrona, L., Norberg, C., and Sunden, B. "Free-stream turbulence and tube spacing effects on surface pressure fluctuations for two tubes in an in-line arrangement," *Journal of Fluids and Structures* Vol. 5, No. 6, 1991, pp. 701-727.

[29]Norberg, C. "Interaction between freestream turbulence and vortex shedding for a single tube in cross-flow," *Journal of wind engineering and industrial aerodynamics* Vol. 23, 1986, pp. 501-514.

[30]Wei, T., and Smith, C. "Secondary vortices in the wake of circular cylinders," *Journal of Fluid Mechanics* Vol. 169, 1986, pp. 513-533.

[31]Bearman, P. "Investigation of the flow behind a two-dimensional model with a blunt trailing edge and fitted with splitter plates," *Journal of fluid mechanics* Vol. 21, No. 2, 1965, pp. 241-255.

[32]Prasad, A., and Williamson, C. H. "The instability of the separated shear layer from a bluff body," *Physics of Fluids* Vol. 8, No. 6, 1996, pp. 1347-1349.

[33]Norberg, C. "LDV-measurements in the near wake of a circular cylinder," *ASME Paper No. FEDSM98-521*, 1998.

[34]Thompson, M. C., and Hourigan, K. "The shear-layer instability of a circular cylinder wake," *Physics of Fluids* Vol. 17, No. 2, 2005, p. 021702.